Applied Surface Science 584 (2022) 152525

Contents lists available at ScienceDirect

Applied Surface Science

journal homepage: www.elsevier.com/locate/apsusc

Full Length Article

A low-fouling, self-assembled, graft co-polymer and covalent surface coating for controlled immobilization of biologically active moieties

Anne-Sophie Mertgen [a,b], Anne Géraldine Guex [a,b], Samuele Tosatti [c], Giuseppino Fortunato [b,1], René M. Rossi [b], Markus Rottmar [a], Katharina Maniura-Weber [a,*], Stefan Zürcher [c,*]

[a] Empa, Swiss Federal Laboratories for Materials Science and Technology, Laboratory for Biointerfaces, Lerchenfeldstrasse 5, 9014 St. Gallen, Switzerland
[b] Empa, Swiss Federal Laboratories for Materials Science and Technology, Laboratory for Biomimetic Membranes and Textiles, Lerchenfeldstrasse 5, 9014 St. Gallen, Switzerland
[c] SuSoS AG, Lagerstrasse 14, 8600 Dübendorf, Switzerland

ARTICLE INFO

Keywords:
Surface Modification
Strain promoted azide-alkyne click chemistry
SPAAC
RGD
Graft copolymer
Cell adhesive surface
Low-fouling

ABSTRACT

Current biointerfaces aiming to steer specific biological responses frequently lack either stability due to purely electrostatic interactions, bioactivity due to unspecific conjugation chemistries, specificity due to uncontrolled biological interactions such as fouling, or cytocompatibility due to harsh and toxic coating procedures. Here, we report a versatile surface modification platform for covalent tethering of selected biomolecules. New in this approach is the particular combination of modular binding blocks as graft co-polymer. Grafted to the backbone of PAcrAm^{TM} multiple functionalities are strategically combined: covalent (silane) and non-covalent (lysine) surface binding groups for stability and self-assembly in mild buffered solution, PEG-azide chains for low fouling properties, and specific, controlled, covalent, linking of biologically active molecules. This modular strategy overcomes the previously mentioned limitations, for instance regarding bioactivity of the biological moiety due to highly specific strain-promoted azide-alkyne cycloaddition. The successful grafting of the copolymer was confirmed by ^{1}H NMR. The immobilization of RGD peptides was characterized by combining surface analytical techniques, such as ToF-SIMS and ellipsometry, allowing quantification of immobilized molecules over an extensive range of concentrations (0.008–1.95 pmol·cm^{-2}). The bioactivity over this range of concentrations was confirmed by *in vitro* cell studies, presenting a differential endothelial cell attachment and spreading. The modified substrates enabled the formation of an interconnected monolayer of endothelial cells. Furthermore, the modular platform allowed the co-immobilization of two bioactive functional groups, RGD and biotin, on the same surface, which could be exploited for the further development of controlled multi-functional biointerfaces for diverse biological applications in the future.

1. Introduction

Biointerfaces that enable controlled and specific interaction with the biological environment that they are exposed to are very critical to overcome current limitations such as in the successful integration of medical implants in the body or biosensing applications [1–3]. For instance, for implant integration creating interfaces that allow steered adhesion of specific cells, which can then perform natural biological functions are desired [4–8]. To this end, adhesion peptides that mediate cell attachment [9] can be immobilized on a synthetic surface [9,10]. Such adhesive peptides are derived from extracellular matrix proteins as for example RGD derived from fibronectin. Additionally, when such cell adhesive functionalization is applied to low-fouling surface coatings, non-specific adsorption of proteins is reduced and non-specific cell interactions with the surface can be avoided [11–14]. Similarly for biosensing applications, in order to obtain high sensitivity, sensor coatings

Abbreviations: PEG, poly(ethylene glycol); PAcrAmTM-g-(PEG-N3NH2,Si), poly(acrylamide)-g-(PEG-N3, 1,6-hexanediamine, 3-amino- propyldimethylsilanol); SPAAC, strain promoted alkyne-azide cycloaddition; DBCO, dibenzocyclooctyne; RGD, arginine-glycine-aspartic acid; ToF-SIMS, time of flight secondary ion mass spectroscopy; VASE, variable angle spectroscopic ellipsometry; ECM, extracellular matrix; HUVEC, human umbilical cord vein endothelial cells.

* Corresponding authors.
E-mail addresses: katharina.maniura@empa.ch (K. Maniura-Weber), stefan.zuercher@susos.com (S. Zürcher).

[1] This author passed away in June 2020.

https://doi.org/10.1016/j.apsusc.2022.152525
Received 1 July 2021; Received in revised form 14 January 2022; Accepted 17 January 2022
Available online 20 January 2022

should avoid any unspecific interaction and therefore be anti-fouling and bioactive in order to capture very specific biomolecules from the analyte [15–18]. For sensing applications, often the high affinity of streptavidin and biotin are exploited [19–21].

In order to create a combined low-fouling and bioactive surface, for instance, poly(ethylene glycol) (PEG) brush-based coatings can be decorated with RGD peptides [22–27]. PEG is an electrically neutral and highly hydrophilic polymer, comprises polar moieties, exhibits hydrogen-bond acceptors, and simultaneously does not present hydrogen-bond donors [28–30]. It thereby enables strong interaction of water molecules *via* hydrogen bonds and thus the formation of a robust hydration layer that entropically and sterically prevents protein adsorption to the underlying material, that can be achieved if densely bound to a surface [30–32]. PEG coatings have been demonstrated on various substrates including but not limited to silicon nitride with silane-PEG or gold with thiol-PEG [33], to diverse negatively charged surfaces by electrostatic adsorption of poly(L-lysine)-*graft*-poly(ethylene glycol) (PLL-*g*-PEG) [34,35], or more recently to silicon oxide by electrostatic and covalent immobilization of poly(acrylamide)-*graft*-(PEG, 1,6-hexanediamine, 3-aminopropyl-dimethylsilanol) (PAcrAm^{TM}-*g*-(PEG,NH_2, Si)) [36]. For the latter, covalent siloxane binding with the silicon oxide surface provides stability while the additional electrostatic binding is required for resilience and achieving optimal packing of the macromolecule on the surface [36]. The reduction of protein adsorption on such coatings strongly depends on the density and length of PEG brushes on the surface. Different grafting densities were previously compared for PLL-*g*-PEG and PAcrAm^{TM}-*g*-(PEG,NH_2,Si), where lowest nonspecific adsorption and thus optimal low-fouling properties could be identified at grafting densities of 0.25 to 0.33 for PLL-*g*-PEG [34,36–38], and of 0.15 for PAcrAm^{TM}-*g*-(PEG,NH_2,Si) [36]. The difference in grafting density for efficient brush formation is being hypothesized to derive from different lengths of backbone repeat units of acrylate and lysine [36]. Furthermore PEG-chain lengths from 2 to 5 kDa have inhibited unspecific protein adsorption [13,17].

PEG based surface coatings have been modified with RGD for instance *via* amide linkage between the N-terminus of the peptide and an acrylated PEG [22,23], or *via* coupling between thiols of functional end group cysteine on the synthetic peptide sequence with either maleimide [27] or vinylsulfone [24–26] functionalized PEG. Even though such RGD functionalization of PEG coatings has been shown to support endothelial cell attachment [11,39,40], amine or thiol-reactive chemistries are not selective [41–43]. Most thiol targeting chemistries also react at a lower affinity with amine groups [41,44,45], and since thiols and amines are abundant in biomolecules [44], these chemistries can impair the biomolecule availability [41]. In contrast, selective immobilization approaches include for instance click chemistries, such as oxime ligation, copper-catalyzed alkyne-azide cycloaddition, or strain-promoted alkyne-azide cycloaddition (SPAAC) [41]. For biomolecule immobilization, in particular, SPAAC is of high interest due to its selective reaction into a triazole ring occurring under mild aqueous conditions and without the need for the addition of potentially toxic metal catalysts [46]. This highly specific reaction between specialized functional groups that do not naturally occur in biomolecules, guarantees the bioavailability of the immobilized molecule [47–49].

Van Dongen et al. [50] developed a PLL-g-PEG version with azide (N_3) end-functionalized PEG chains, which enabled the covalent immobilization of bicyclononyne-conjugated RGD peptide *via* SPAAC and allowed for the controlled attachment of HeLa cells [50]. However, PLL-g-PEG-N_3 is relying only on electrostatic adsorption to the surface and thus lacks long-term stability under ion-rich physiological conditions.

Here we present an azido-PEG coating based on a graft copolymer with a PAcrAm^{TM} backbone, that in contrast to the previous coating strategies combines hexanediamine sidechains for electrostatic adsorption for resilience and aminopropyldimethylsilanol side chains for improved stability *via* covalent bonding to silicon-based surfaces. Furthermore, this low-fouling platform was combined with selective SPAAC immobilization of a dibenzocyclooctyne (DBCO)-conjugated biomolecules. Here, DBCO-RGD surface concentration was tuned by peptide solution concentration during SPAAC immobilization, and surfaces were characterized by ToF-SIMS and ellipsometry. Endothelial cell attachment and spreading were assessed as a function of RGD surface concentration, and an interconnected endothelial monolayer could be obtained at high RGD densities. The surface modification platform was further explored for co-immobilization of RGD with a second bioactive molecule, here biotin, and showed uncompromised bioactivity of both molecules. Overall, the proposed covalent, low-fouling, and bioactive coating, which enables the selective and concentration-controlled immobilization of biomolecules, bears the potential for prospective use for coating implant materials or biosensing applications.

2. Experimental

2.1. Materials

Toluene (analytical grade), 2-propanol (analytical grade), N,N-dimethylformamide (DMF, ≥99.8%), dichloromethane (DCM, 99+%), diethyl ether (Et_2O, analytical grade), trifluoroacetic acid (TFA, analytical grade), and triethylamine (NEt_3, analytical grade) were purchased from Merck, Switzerland; 4-(2-Hydroxyethyl)piperazine-1-ethanesulfonic acid (HEPES, ≥99%) was from BDH Biochemical, USA. Sodium chloride (NaCl, ≥99.5%), phosphate-buffered saline (PBS, pH 7.4), penicillin/streptomycin/neomycin (PSN) and dibenzocyclooctyne-PEG4-biotin conjugate (DBCO-biotin), 3-(ethoxydimethylsilyl)propylamine, N-Boc-1,6-hexanediamine hydrochloride (≥98%), and deuterium oxide (99.9 at.% D) for NMR spectroscopy were obtained from Sigma Aldrich, Switzerland; lyophilized streptavidin was purchased from iba Lifesciences, Germany. Streptavidin-horseradish peroxidase (streptavidin-HRP, 50 μg·mL^{-1}) solution, 3,3′,5,5′-tetramethylbenzidine (TMB) substrate, and 450 nm stop solution were obtained from Abcam, Switzerland. Silicon wafer chips, $9 \times 10\ mm^2$ were acquired from Powatec GmbH, Switzerland. Peptides DBCO-RGD (DBCO-mal-CKK-(aminocaproic acid)$_3$-GRGDS) and DBCO-RDG (DBCO-mal-CKK-(aminocaproic acid)$_3$-GRDGS) were custom-synthesized by Chinapeptides Ltd., China, and provided at 95% purity (KK was used to maintain the hydrophilicity of the peptide next to a hydrophobic aminocaproic acid spacer). Streptavidin-AlexaFluor®430 conjugate, phenol red-free M200 cell culture medium, low serum growth supplement (LSGS) as well as pooled human umbilical cord vein endothelial cells (pHUVEC) were purchased from Thermo Fisher, Switzerland. Tissue culture flasks and well plates were obtained from Techno Plastic Products AG, TPP, Switzerland. HEPES buffers used throughout the experiments were prepared according to HEPES 0 buffer (1 mM HEPES, pH 7.4); HEPES I buffer (10 mM HEPES, pH 7.4), and physiological HEPES II buffer (10 mM HEPES, 150 mM NaCl, pH 7.4). Poly(pentafluorophenyl acrylate) (pPFPAc) ($M_w = 238.18\ g{\cdot}mol^{-1}$ monomer, DP = 100) was synthesized as previously published [36]. α-Azido-ω-ammonium trifluoroacetate poly(ethyleneglycol) (N_3-PEG-$NH_3^+CF_3COO^-$) $M_w = 3500\ g{\cdot}mol^{-1}$ was obtained from JenKem Technology Inc., USA, and ultrapure water (purified with a water-treatment apparatus from Millipore, ≥18.2 MΩ cm-1 resistivity, total organic content ≤ 5 ppb) was used throughout the experiments (Merck Millipore, Switzerland).

2.2. Polymer synthesis and characterization

The synthesis of the graft copolymer poly(acrylamide)-g-(PEG-N_3, 1,6-hexanediamine, 3-amino- propyldimethylsilanol) (7000:350 0:116.2:161.3 M *ratio*; 0.15:0.425:0.425 *d*) (PAcrAm^{TM}-*g*-(PEG-N_3, NH_2, Si) was carried out following the previously published procedure for the corresponding PEG version [36]. A solution of N_3-PEG-$NH_3^+CF_3COO^-$ (452 mg, 0.126 mmol) in 4.5 mL of DMF together with NEt_3 (98 μL, 0.7 mmol) was prepared under stirring and added dropwise

to another solution of pPFPAc (200 mg, 0.839 mmol of monomer) in 2 mL of DMF. The mixture was stirred overnight at 50 °C. N-Boc-1,6-hexanediamine hydrochloride (90.1 mg, 0.356 mmol) was dissolved in 1 mL of DMF together with NEt_3 (110 µL, 0.799 mmol) and added dropwise to the resulting PAcrAm-*g*-(PEG-N_3, PFPAc) solution. The resulting clear solution was left to react overnight under stirring at 50 °C. A solution of 3-aminopropyldimethylethoxysilane (141 µL, 0.749 mmol, excess) and NEt_3 (207 µL, 1.490 mmol) was added to the above solution and left to react overnight under stirring at 50 °C. DMF was removed under reduced pressure, and the crude product was dissolved in 10 mL of DCM to obtain a brown solution. TFA (2.5 mL) was added, and the mixture was stirred overnight at room temperature. The solvents were evaporated under reduced pressure, and the crude oily material was extracted with 2 times 20 mL of Et_2O and dispersed in 10 mL of ultrapure water. NaOH solution (1 M, 0.5 mL) was added to obtain a clear solution, which was dialyzed (3.5 kDa MWCO membrane) for 2 days against ultrapure water. The polymer was filtered (0.2 µm pore size) and isolated by freeze-drying as an off-white fluffy powder. Yield: 441 mg. ^{1}H NMR (300 MHz, D_2O): δ[ppm] 4–3.2 ($-CH_2CH_2-$ in PEG polymer chains), 3.2–2.6 (broad signals from the PAcrAm backbone, $-CH_2-NH_3+$ and $-NH-CH_2-$), 2.2–1.75 (broad signals from the PAcrAm backbone) 1.55, 1.45, and 1.30 (broad signals from $-CH_2-$ of hexylamine and silane side chains), 0.52 ($-CH_2-Si(CH_3)_2OH$), and 0.07 ($-CH_2-Si(CH_3)_2OH$). The estimated molecular weight of this polmer is calculated to be 68 kDa.

The reference polymer PAcrAm^{TM}-*g*-(PEG,NH_2,Si) (7000:2000:116.2:161.3 M *ratio*; 0.15:0.425:0.425 *d*) was synthesized as described previously [36].

2.3. Polymer coating and characterization

Silicon wafer chips with a natural oxide layer were used as substrates for all experiments. Wafers were cleaned by sonication in toluene (two times, 10 min) followed by sonication in 2-propanol (two times, 10 min) and subsequently dried under nitrogen. After oxygen plasma cleaning for 2 min, the oxide layer thickness was measured with variable angle spectroscopic ellipsometry (VASE). Next, samples were immersed in 0.1 mg·mL^{-1} PAcrAm^{TM}-*g*-(PEG-N_3,NH_2,Si) or PAcrAm^{TM}-*g*-(PEG,NH_2, Si) in HEPES 0 solution for 30 min. After cleaning three times in ultrapure water and drying under nitrogen, the thickness of the adsorbed polymer layer was measured by VASE. Loosely adsorbed polymer was removed by incubation in HEPES II overnight. The remaining stable polymer layer was measured again after three times washing in ultrapure water and drying under nitrogen.

2.4. Protein adsorption

Protein adsorption resistance of PAcrAm^{TM}-*g*-(PEG-N_3,NH_2,Si), PAcrAm^{TM}-*g*-(PEG,NH_2,Si), or uncoated reference samples was evaluated by incubation of samples in M200 medium serum supplemented with low serum growth supplement including 2% fetal bovine serum for 30 min. After washing three times in HEPES II, three times in ultrapure water, and drying under nitrogen, the adsorbed protein layer thickness was measured by VASE.

2.5. RGD or biotin functionalization

Different concentrations of DBCO-biotin or DBCO-RGD were immobilized on PAcrAm^{TM}-*g*-(PEG-N_3,NH_2,Si) by immersing samples in solutions of different concentrations (0 µM to 100 µM) for 60 min. Samples were washed three times in HEPES II, three times in ultrapure water, and dried under nitrogen. The immobilization was characterized by Time of Flight - Secondary Ion Mass Spectroscopy (ToF-SIMS) and in the case of RGD functionalization additionally by VASE.

2.6. Sequential co-immobilization of RGD and biotin

In order to investigate if the proposed platform allows for co-immobilization of at least two different bioactive molecules on the same substrate without compromising their bioactivity, the sequential immobilization of RGD and biotin was explored as proof of concept. Biotin was chosen as a well-known biomolecule that allows detection independently from RGD using VASE, ToF-SIMS, a fluorescence assay with HRP-streptavidin or fluorescently labelled streptavidin. To this end, first, only RGD was immobilized at a low concentration of 0.3 µM to guarantee that a sufficient number of azide groups are available for the subsequent biotin immobilization in a second step at a solution concentration of 30.9 µM. A sample with four differently functionalized areas was created by first immersing half of the sample in DBCO-RGD solution followed by washing (three times with HEPES II and three times with ultrapure water), drying under nitrogen and rotating the sample 90° and secondly by immersing the orthogonal other half in DBCO-biotin solution. The resulting four different zones on the same sample were: (1) PAcrAm^{TM}-*g*-(PEG-N_3,NH_2,Si), (2) RGD functionalization only, (3) biotin functionalization only and (4) combination of RGD and biotin functionalization (Fig. 5B). These patchwork samples were analyzed by surface chemical ToF-SIMS and for their bioactivity by either analysis of HUVEC attachment (N = 3 individual experiments, n = 2 technical repeats) or probing with fluorescently labeled streptavidin (N = 3, n = 2). For streptavidin labeling of biotin, samples were incubated in 1:200 streptavidin-AlexaFluor®430 in PBS for 60 min. After washing three times in PBS, the samples were imaged with a confocal laser scanning microscope (CLSM, LSM780, Zeiss, Germany).

2.7. Time of flight – Secondary ion mass spectroscopy (ToF-SIMS)

Chemical characterization of the coating was performed with a Tof-SIMS 5 instrument (IONTOF, Germany), operated in spectrometry configuration mode. This mode used pulsed 25 keV Bi_3^{++} primary ions in a high mass resolution mode at a pressure below 5×10^{-8} mbar in static mode to allow the analysis of the uppermost few nanometers of the coating. Negatively charged secondary ions from mass 1 to 880 u were measured in a ToF analyzer with a sensitivity in the ppm range. Two to four randomly selected areas of 200 × 200 µm^2 (128 × 128 pixels^2) were analyzed per sample to obtain statistically relevant results. Each measurement was set to 180 s while various scans were acquired. (N = 2 (biotin) or N = 3 (RGD), n = 2). One patchwork sample from sequential RGD and biotin immobilization was analyzed by acquiring single spectrum measurements in each area and additionally with an area scan of 5 × 5 mm^2 (500 × 500 pixels^2) (N = 1).

For the comparison of the signal intensities of relevant chemical fragments derived from DBCO-RGD and DBCO-biotin (S- derived from cysteine amino acid (peptide sequence) or biotin and $C_{16}H_{11}N$- from DBCO) were shown as integrated peak area in the spectrum (=integrated signal intensity).

2.8. Variable angle spectroscopic ellipsometry (VASE)

The dry layer thickness at different coating steps was measured with an M−2000F variable-angle spectroscopic ellipsometer (J. A. Woollam Co., Inc., USA). Measurements were recorded using an incidence angle of 70° in the spectral range of 370 to 1000 nm and under ambient conditions. The recorded data were fitted with a Cauchy multilayer model (A = 1.45, Bn = 0.01, Cn = 0) using custom analysis software (Complete EASE, J.A. Woollam Co. Inc., USA) for modeling the optical thickness of the adlayers. (N = 3 (RGD, streptavidin) or N = 5 (PAcrAm^{TM}-*g*-(PEG-N_3,NH_2,Si)), n = 3).

2.9. Theoretical calculations

Surface concentrations of PEG-N_3 (3500 g·mol^{-1}), RGD

(1616.6 g·mol^{-1}) or streptavidin (60·10^3 g·mol^{-1}) layers were calculated using dry mass densities of 1.3 g·cm^{-3} for peptides and proteins [51–53] and 1.17 g·cm^{-3} for PEG polymer [54] and the following equation (Eq. (1)):

$$\frac{c}{A} = \frac{t^*\rho}{M_w} * 10^5 \quad (1)$$

with M_w = molecular weight (g·mol^{-1}), c = concentration (pmol), ρ = dry mass density (g·cm^{-3}), t = layer thickness (nm) and A = area (cm^2). In order to obtain a generic relationship between solution concentration and surface concentration of RGD immobilization, the obtained VASE derived concentration data were fitted to the following equation for irreversible binding (Eq. (2)) [55]:

$$\frac{c}{A} = \frac{B_{max} * x}{K_{1/2} + x} \quad (2)$$

with c/A = concentration per area (pmol·cm^{-2}), $K_{1/2}$ = equilibrium binding constant or the solution concentration (μM), at which half of the available binding sites are occupied after 1 h incubation, x = the evaluated or used solution concentration (μM) and B_{max} = the maximum of available binding sites per area (pmol·cm^{-2}). To estimate the PEG-N_3 concentration, the calculated concentration obtained from Eq.2 was multiplied with the ratio $r_{PEG\text{-}N3}$ (Eq. (3)) in order to account for the fraction of PEG-N_3:

$$r_{PEG-N3} = \frac{b * M_{w,PEG-N3}}{b * M_{w,PEG-N3} + a * M_{w,NH2} + c * M_{w,Si} + 1 * M_{w,acrylamide}} \quad (3)$$

with r = ratio, a,b,c = grafting densities (see Fig. 1A) and M_w = molecular weight (g·mol^{-1}). The distance (spacing) between RGD peptides was computed according to equation (Eq. (4)) [24]:

$$d_{RGD-RGD}(nm) = \sqrt{\left(\frac{2}{\sqrt{3}} * \frac{1}{c/A * N_A}\right)} * 10^7 \quad (4)$$

with d = distance (nm), c/A = concentration per area (pmol·cm^{-2}), N_A = Avogadro constant (6.022·10^{23} mol^{-1}).

2.10. Endothelial cell culture

Pooled human umbilical cord vein endothelial cells (pHUVECs, Thermo Fisher, Switzerland) were cultured in M200 medium supplemented with LSGS and 1% (v/v) PSN in gelatin-coated (coated with 1% (w/v) gelatin in ultrapure water for 10 min) tissue culture flasks. Cells

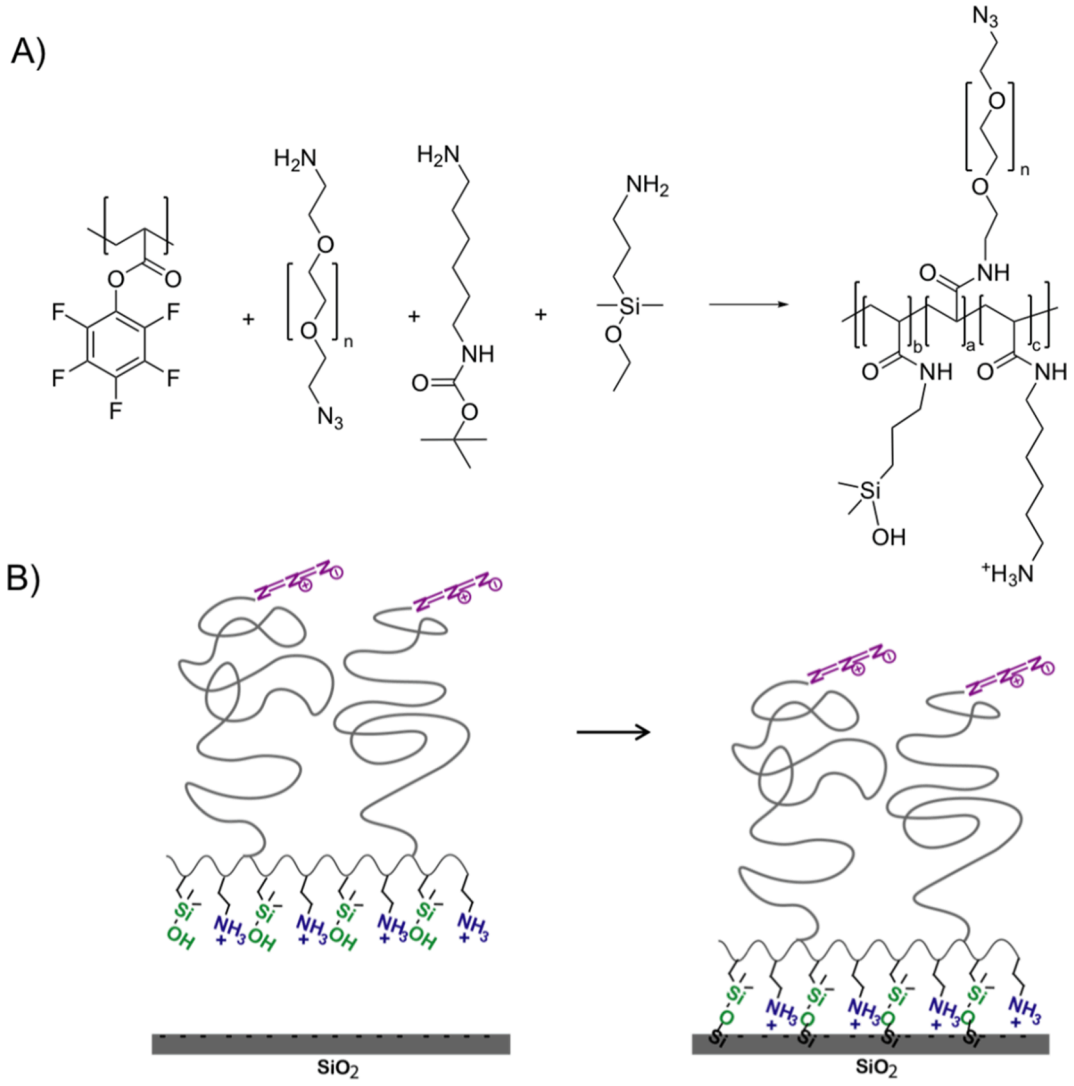

Fig. 1. (A) Scheme for the synthesis of PAcrAm^{TM}-*g*-(PEG-N_3,NH_2,Si) with stoichiometric grafting densities of a = 0.15, b = 0.425 and c = 0.425; (n = 80). (B) In the simplified representation of the molecule, the PEG chain is illustrated in grey, the azide in purple, and Si or NH_2 in green or blue, respectively. The electrostatic (NH_3^+ at pH 7.4) and the covalent (siloxane bonding) immobilization of PAcrAm^{TM}-g-(PEG-N_3,NH_2,Si) on the SiO_2 wafer is illustrated. (For interpretation of the references to colour in this figure legend, the reader is referred to the web version of this article.)

were subcultured at 90% confluency at a ratio of 1:5 and used for experiments up to passage 8.

2.11. Endothelial cell attachment on RGD-functionalized samples and immunofluorescence imaging

pHUVEC were trypsinized and harvested in LSGS supplemented M200 medium. After centrifugation at 180g, the cell pellet was suspended in serum free M200 medium. Cells were seeded at a concentration of $1.6x10^5$ cells·cm^{-2} and cultured in serum free conditions at 5% CO_2 and 37 °C. In order to analyze early RGD specific attachment and spreading, samples were harvested after 4 h and fixed in 4% (v/v) paraformaldehyde in PBS for 15 min.

For analysis of endothelial monolayer formation over 3 days, serum containing medium was added after 4 h of serum free culture as described before, and samples were incubated at 5% CO_2 and 37 °C for 3 days. On day 3, cells were fixed in 4% (v/v) paraformaldehyde in PBS for 15 min.

Prior to immunostaining, cells were permeabilized with 0.1% (v/v) triton-X in PBS for 30 min and blocked in 2% (w/v) bovine serum albumin (BSA) in PBS for 60 min. Samples were then stained for nuclei with 1:1000 4′,6-diamidino-2-phenylindole (DAPI, Thermo Fisher, Switzerland) and actin skeleton with 1:200 phalloidin-AlexaFluor®488 (Thermo Fisher, Switzerland) in 2% (w/v) BSA in PBS for 30 min. After subsequent washing with PBS samples were imaged with a fluorescence microscope (Axio Imager M1, Zeiss, Germany) or a confocal laser scanning microscope. For visualization of endothelial monolayer integrity after 3 days, samples were additionally stained for VE-cadherin with 1:500 rabbit VE-cadherin antibody (Cell Signaling Technology, Netherlands) in 2% (w/v) BSA in PBS at 4 °C overnight. After washing with PBS, samples were incubated in 1:200 anti-rabbit antibody conjugated to AlexaFluor®555 (Thermo Fisher, Switzerland) in 2% (w/v) BSA in PBS for 1 h at room temperature. After subsequent washing with PBS samples were imaged with a confocal laser scanning microscope.

Cell spreading and cell numbers were quantified by image analysis with ImageJ (https://imagej.nih.gov/ij/download.html). Cell numbers were quantified by applying particle counting on cell nuclei (DAPI) images. Cell spreading was evaluated by measuring the area stained positively for actin per image relative to the cell number of the same image. The macro codes for automatic particle counting and actin area quantification are provided in the supplementary material. (N = 3, n = 3).

2.12. Evaluation of biotin functionality

The functionality of biotin after immobilization was verified by incubation in 0.48 nM streptavidin-HRP in PBS for 60 min. After washing three times in PBS the streptavidin-HRP binding was evaluated by determining the enzymatic activity *via* enzyme-linked immunosorbent assay (ELISA). To this end, samples were placed in a fresh well plate. They were incubated in TMB substrate on a shaker for 10 min before the enzymatic conversion was stopped by adding an equal amount of 450 nm stop solution. The absorbance of the resulting solution was measured at 450 nm. (N = 3, n = 3).

2.13. Statistical analysis.

GraphPad Prism 8 was used for all statistical analyses and plotting of graphs. For analysis of statistically significant differences between groups, a nonparametric Mann-Whitney test was used to compare ranks with a significance level of $p < 0.05$. The relationships between x and y throughout different experiments were fitted with a one-side specific binding equation (*Eq. (2)*) or linear relationship. The precision of the fit is reported with R^2. The Pearson correlation factor R^2 between ligand spacing and cell response was reported with a significance level of $p < 0.05$.

3. Results

3.1. PAcrAm^{TM}-g-(PEG-N$_3$,NH$_2$,Si) synthesis and analysis of coating stability and protein adsorption

For the synthesis of PAcrAm^{TM}-g-(PEG-N$_3$,NH$_2$,Si) and reference polymer PAcrAm^{TM}-g-(PEG,NH$_2$,Si), the different amine-functional sidechains were attached by sequential stoichiometric grafting to the amine- reactive pPFPAc backbone (Fig. 1A) as described in previous publications [36,56]. The same grafting densities of $a_{PEG\text{-}N3} = 0.15$ (optimal for reducing protein adsorption) [36], $b_{Si} = 0.425$ and $c_{NH2} = 0.425$ were used for both polymers but longer PEG chains were attached for PAcrAm^{TM}-g-(PEG-N$_3$,NH$_2$,Si) ($M_{w,PEG\text{-}N3} = 3500$ g·mol^{-1} vs $M_{w,PEG} = 2000$ g·mol^{-1}). In the ^{1}H NMR spectrum signals for all sidechains could be clearly detected, indicating successful polymer synthesis (Fig. S1).

Silicon wafers exhibiting a thin silicon oxide layer (SiO_2) were coated with PAcrAm^{TM}-g-(PEG-N$_3$,NH$_2$,Si) or PAcrAm^{TM}-g-(PEG,NH$_2$,Si) polymers. (Schematic of coating shown in Fig. 1B) The dry layer thickness of the adsorbed polymer immediately after coating was increased for PAcrAm^{TM}-g-(PEG-N$_3$,NH$_2$,Si) (2.12 ± 0.11 nm) compared to control PAcrAm^{TM}-g-(PEG,NH$_2$,Si) (1.86 ± 0.10 nm) ($p < 0.05$) (Table 1). However, after incubation in HEPES II buffer overnight for removal of non-covalently bound molecules, and after rinsing and drying, the stable dry layer thickness of both coatings was determined with an average value of 1.56 ± 0.11 or 1.56 ± 0.10 nm, respectively (Table 1). From the layer thickness of PAcrAm^{TM}-g-(PEG-N$_3$,NH$_2$,Si) the azide concentration was calculated according to *Eq. (1) and (3)* as c(N$_3$) = 38.9 ± 2.7 pmol·cm^{-2}.

After immersion of the surfaces in serum supplemented cell culture medium, protein adsorption on uncoated SiO_2 wafers, PAcrAm^{TM}-g-(PEG-N$_3$,NH$_2$,Si) and PAcrAm^{TM}-g-(PEG,NH$_2$,Si) coated wafers was measured as dry layer thickness. No significant change in layer thickness was observed on both PAcrAm^{TM}-g-(PEG-N$_3$,NH$_2$,Si) ($p = 0.16$) and PAcrAm^{TM}-g-(PEG,NH$_2$,Si) ($p = 0.49$) coatings, whereas on uncoated SiO_2 reference an adlayer thickness of 3.34 ± 0.63 nm was determined (Table 1).

3.2. Concentration controlled RGD immobilization on PAcrAm^{TM}-g-(PEG-N$_3$,NH$_2$,Si) via strain promoted cycloaddition

The ability of the azide end-group to perform strain promoted cycloaddition with DBCO-conjugated RGD peptide (Fig. 2A) to form a covalent triazole ring (Fig. 2B) in a concentration-controlled manner was investigated by incubating PAcrAm^{TM}-g-(PEG-N$_3$,NH$_2$,Si) coated substrates in DBCO-RGD solutions at various concentrations (0 to 100 µM). The modified surfaces were analyzed by ToF-SIMS and the integrated signal intensity of two peptide specific fragments (S^- derived from cysteine in the peptide sequence and $C_{16}H_{11}N^-$ originating from the DBCO group) were determined as function of solution concentration.

Table 1
Polymer immobilization and protein resistance analysis *via* layer thickness evaluation with VASE.

	Thickness of adsorbed polymer layer (30 min) (nm)	Thickness of polymer layer after immersion in HEPES II overnight (nm)	Thickness of adsorbed polymer and protein layer after incubation in serum supplemented medium (30 min) (nm)
PAcrAm^{TM}-g-(PEG-N$_3$, NH$_2$,Si)	2.12 ± 0.11	1.56 ± 0.11	1.51 ± 0.04
PAcrAm^{TM}-g-(PEG,NH$_2$, Si)	1.86 ± 0.10	1.56 ± 0.10	1.59 ± 0.08
SiO_2 reference	n.a.	n.a.	3.34 ± 0.63

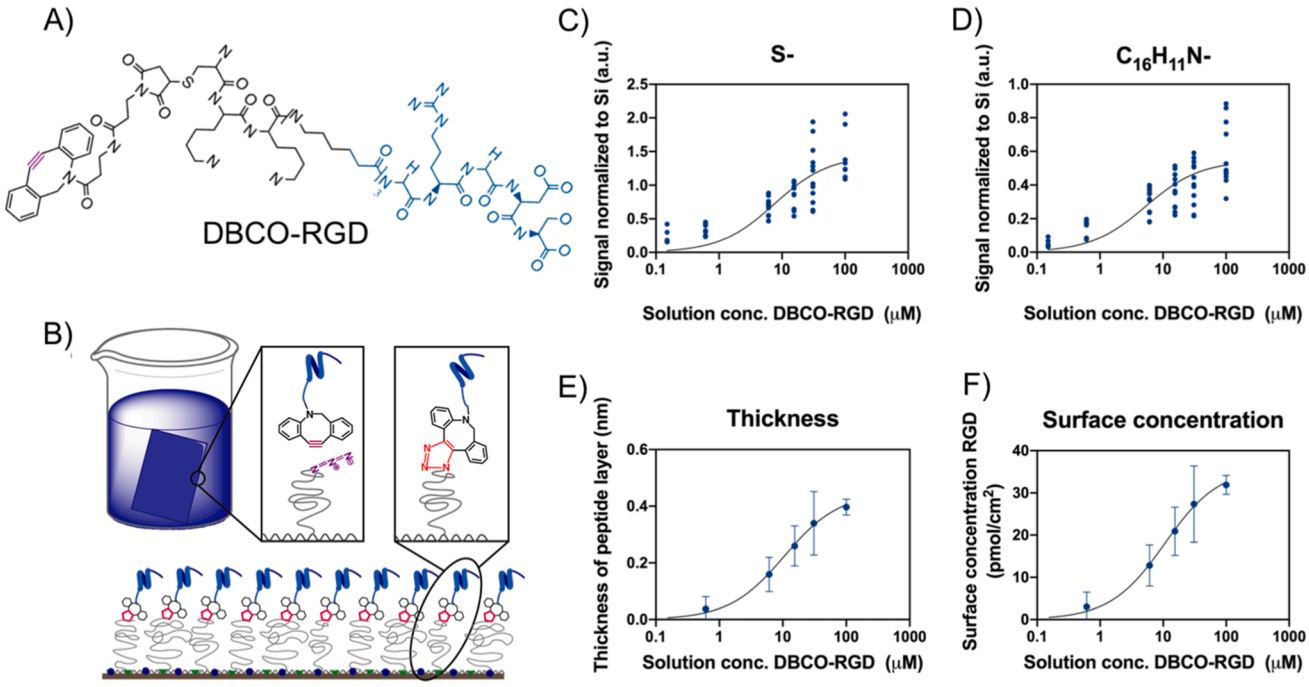

Fig. 2. SPAAC based immobilization of DBCO-RGD. (A) Chemical structure of DBCO-RGD. (B) During incubation of PAcrAm^{TM}-*g*-(PEG-N_3,NH_2,Si) coated samples in DBCO-RGD solutions (beaker), the azide functionality on PAcrAm^{TM}-*g*-(PEG-N_3,NH_2,Si) coating and the alkyne of the DBCO (left scheme) form a covalent triazole ring (right scheme). Chemical characterization of RGD surface concentration was achieved *via* ToF-SIMS: Integrated signals from S^- (C) or $C_{16}H_{11}N^-$ (D) peaks. (N = 3, n = 2) VASE based analysis of RGD peptide layer thickness (E) allowed the calculation of RGD surface concentration (F) according to *Eq. (1)* (N = 3, n = 3).

The intensity increased with rising RGD solution concentration following *Eq. (2)* (S-: $R^2 = 0.68$, $C_{16}H_{11}N$-: $R^2 = 0.67$) (Fig. 2C and 2D). Similarly, VASE measurements showed increasing layer thickness of DBCO-RGD immobilized on PAcrAm^{TM}-*g*-(PEG-N_3,NH_2,Si) according to *Eq. (2)* ($R^2 = 0.83$) (Fig. 2E). The RGD layer thickness allowed the computation of surface concentration according to *Eq. (1)* (Fig. 2F). Notably, the limit of detection for ToF-SIMS (0.15 μM DBCO-RGD solution concentration) was 40 times lower compared to VASE (6.1 μM DBCO-RGD solution concentration).

By fitting the computed RGD surface concentration to *Eq. (2)* $K_{1/2}$ and B_{max} parameters were derived (Table 2). A second model was generated for comparison by combining $K_{1/2}$ derived from ToF-SIMS $C_{16}H_{11}N^-$ data with the azide surface concentration c(N_3) (38.9 pmol·cm^{-2}) as B_{max} (Table 2).

3.3. Analysis of RGD concentration dependent endothelial cell attachment and spreading and endothelial monolayer formation

The RGD concentration dependent cell response was shown by endothelial cell seeding and observation of their spreading after 4 h in serum free condition. The number of cells and their spreading increased with increasing RGD concentration from 0.008 to 1.95 pmol·cm^{-2} as shown qualitatively by immunofluorescence imaging in Fig. 3A and quantitatively as nuclei count and actin area per cell in Fig. 3B.

Table 2
Parameters of fitting data derived from VASE and ToF-SIMS analysis to *Eq. (2)*. In the case of ToF-SIMS B_{max} is assumed to be the azide surface concentration determined from VASE ((*)B_{max} = c(N_3)).

Data used for fitting	$K_{1/2}$ (μM)	B_{max} (pmol·cm^{-2})	Coefficient of determination (R^2)
c(RGD) (VASE)	10.6	36.0	0.85
$C_{16}H_{11}N$- RGD (ToF-SIMS)	5.3	38.9*	0.67
$C_{16}H_{11}N$- biotin (ToF-SIMS)	54.9	38.9*	0.84

Unmodified PAcrAm^{TM}-*g*-(PEG-N_3,NH_2,Si) coated surfaces or substrates modified with scrambled DBCO-RDG peptide prevented any cell attachment (Fig. 3A and C). After three days of cell culture on RGD modified substrates (1.95 pmol·cm^{-2}) in serum containing condition, a confluent monolayer of endothelial cells was achieved shown by full coverage of the surface. VE-cadherin was stained as a marker for the endothelial cell specific inter-cellular adherens junctions between cells and was positive as shown in Fig. 3D and Fig. S4.

3.4. Sequential co-immobilization of RGD and biotin for dual functional surfaces

First, for establishing the immobilization of a second model biomolecule, biotin was used in order to exploit the affinity with streptavidin for subsequent bioavailability testing. DBCO-conjugated biotin (Fig. 4A) was immobilized on PAcrAm^{TM}-*g*-(PEG-N_3,NH_2,Si) (Fig. 4B) at the same molar solution concentrations as DBCO-RGD. The immobilization was subsequently evaluated by surface chemical ToF-SIMS analysis where sulfur (S^-) fragments are derived from the biotin and the $C_{16}H_{11}N^-$ fragment is derived from DBCO.

The integrated signal intensity of S^- and $C_{16}H_{11}N^-$ fragments correlated with rising solution concentration for biotin according to *Eq. (2)* (S^-: $R^2 = 0.93$, $C_{16}H_{11}N^-$: $R^2 = 0.94$) (Fig. 4C,D). The limit of detection was 0.61 μM of DBCO-biotin solution concentration. Generally, no evidence of unspecific immobilization of DBCO-biotin on PAcrAm^{TM}-*g*-(PEG,NH_2,Si) coated samples was observed (Fig. S2).

As previously described for RGD, to estimate the biotin surface concentrations, the $K_{1/2}$ derived from ToF-SIMS $C_{16}H_{11}N^-$ data fitted to *Eq. (2)*, was combined with the azide surface concentration c(N_3) (38.9 pmol·cm^{-2}) as B_{max} (Table 2). From these data we could observe, that the binding kinetics for DBCO-biotin differ from the ones of DBCO-RGD. After 1 h of immobilization, the $K_{1/2,ToF\text{-}SIMS,RGD}$ (5.3 μM) was lower than $K_{1/2,ToF\text{-}SIMS,biotin}$ (54.9 μM) by a factor or 10, which indicates a faster binding of the RGD functionalized DBCO.

The availability of biotin after immobilization was investigated by affinity binding of HRP conjugated streptavidin to the biotin modified

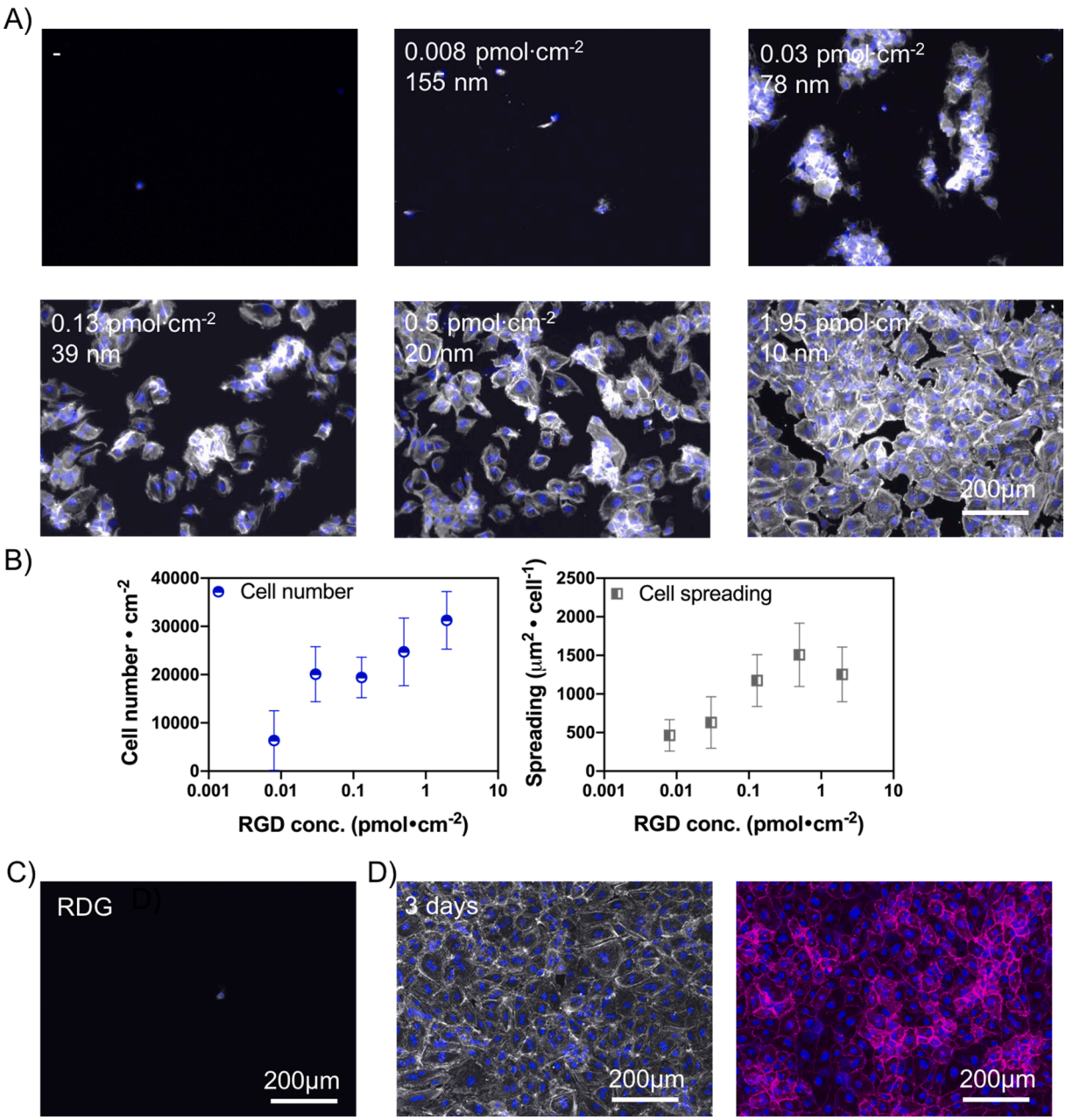

Fig. 3. HUVEC attachment and spreading was analyzed in response to RGD concentration immobilized to PAcrAm^{TM}-g-(PEG-N_3,NH_2,Si). (A) The attachment of HUVEC on surfaces with different RGD concentrations (0 – 1.95 pmol·cm^{-2}) after 4 h in serum free conditions was visualized by immunofluorescence staining of nuclei (blue) and actin skeleton (white). (N = 3, n = 3) (B) Cell number (nuclei counts) and spreading (actin area per cell) was quantified with ImageJ based image analysis. (N = 3, n = 3) (C) As control, HUVEC attachment on surfaces functionalized with scrambled RDG peptide was analyzed. (N = 3, n = 3) (D) After 3 days of cell culture in serum supplemented media, HUVECs were visualized by immunofluorescence staining of nuclei (blue), actin skeleton (white) and VE-cadherin (pink). (N = 3, n = 3).

surfaces and subsequent evaluation by ELISA. Using this sensitive readout, streptavidin-HRP concentration was increasing together with rising biotin concentrations following *Eq. (2)* ($R^2 = 0.87$) as shown in Fig. 4E.

As a proof of concept for co-immobilization of at least two different bioactive molecules on the same substrate without compromising their bioactivity, the sequential (not competitive) immobilization of DBCO-RGD and DBCO-biotin to PAcrAmTM-g-(PEG-N3,NH2,Si) coated surfaces was explored (Fig. 5A). Samples with four differently functionalized areas were created as described in the methods: (1) PAcrAm^{TM}-g-(PEG-N_3,NH_2,Si) background, (2) biotin only, (3) RGD and biotin and (4) RGD only (Fig. 5B). The solution concentration of 0.3 µM of DBCO-RGD was chosen to obtain a low RGD surface density of<10 pmol.cm^{-2} leaving more than 30 pmol.cm^{-2} functional azides on the surface to obtain a high biotin surface concentration after the subsequent DBCO-biotin immobilization. A ToF-SIMS area scan of $C_{16}H_{11}N^-$ fragment intensities exhibited a visible difference between areas 1 and 4 and biotin functionalized areas 2 and 3 due to high biotin concentration (Fig. 5C). ToF-SIMS spectra taken from each area confirmed this observation by increased integrated signal intensities from S^- and $C_{16}H_{11}N^-$ fragments especially in biotin covered area 2 (S^-: 0.32, $C_{16}H_{11}N^-$: 0.17) and area 3 (S^-: 0.38, $C_{16}H_{11}N^-$: 0.2) but also in RGD covered area 4 (S: 0.15, $C_{16}H_{11}N$-: 0.04) compared to area 1 (S^-: 0.08, $C_{16}H_{11}N^-$: 0.00)(Fig. 5D). By binding of fluorescently labeled streptavidin to biotin and subsequent fluorescence imaging, a homogeneous fluorescence signal was observed on areas 2 and 3, indicative for biotin functionalization (Fig. 5E).

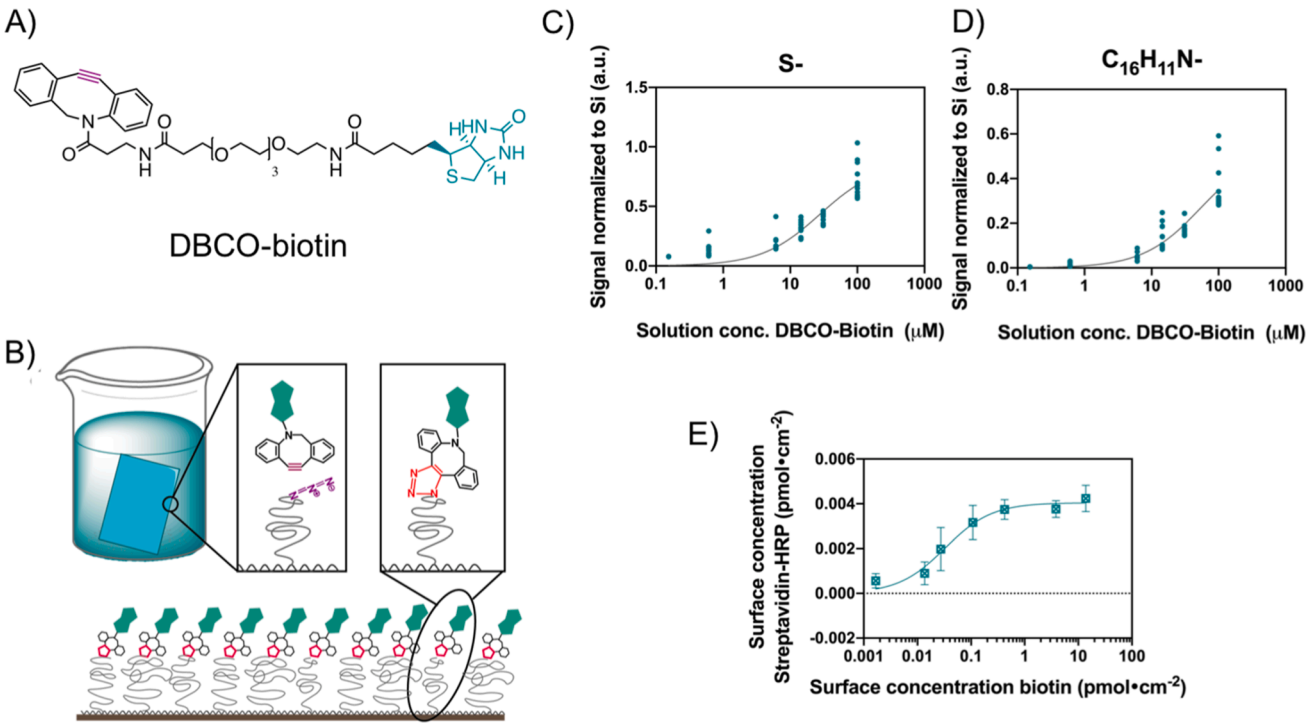

Fig. 4. SPAAC based immobilization of DBCO-biotin. A) Chemical structure of DBCO-biotin. B) During incubation of PAcrAm^{TM}-*g*-(PEG-N_3,NH_2,Si) coated samples in DBCO-biotin solutions (beaker), the azide functionality on PAcrAm^{TM}-*g*-(PEG-N_3,NH_2,Si) coating and the alkyne of the DBCO (left magnification) form a covalent triazole ring on the coating (right magnification). Chemical characterization of biotin surface concentration was achieved *via* ToF-SIMS: Integrated signals from S^- (C) or $C_{16}H_{11}N^-$ (D) peaks. (N = 2, n = 2) E) Streptavidin binding to biotin was quantified using an adapted ELISA assay, by incubating biotin functionalized surfaces in HRP conjugated streptavidin solution and subsequently measuring the HRP derived enzymatic activity. (N = 3, n = 3).

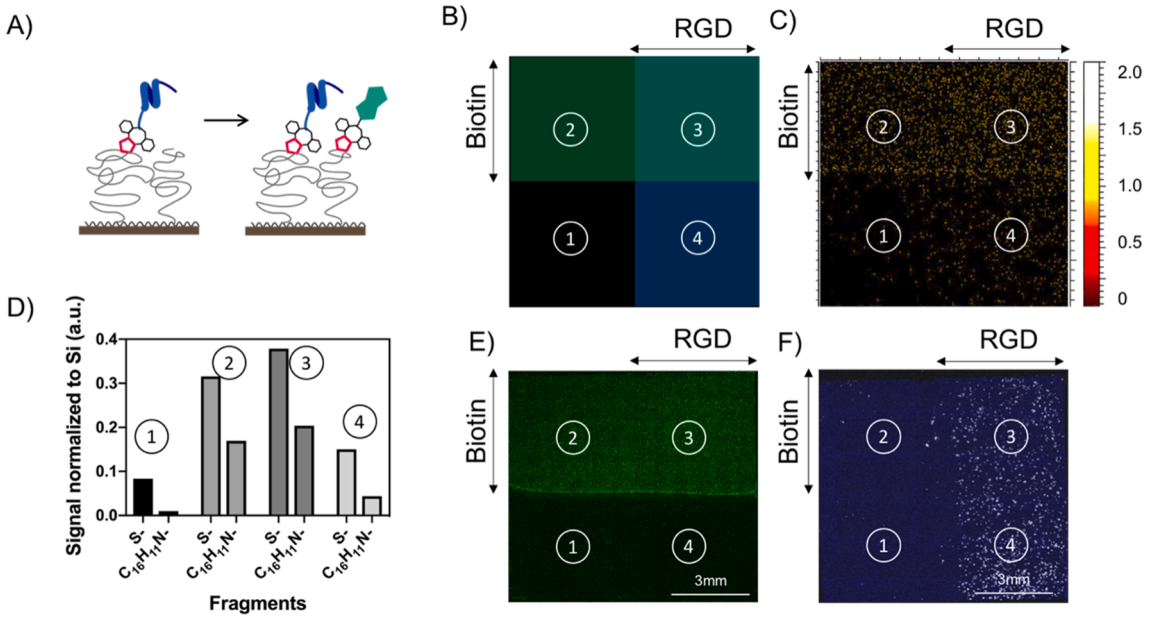

Fig. 5. Sequential dual functionalization of surfaces with RGD and biotin. (A) Schematic of sequential co-immobilization of first RGD (blue) and secondly biotin (green). (B) By functionalizing half of the sample with green and blue mixed-up here as indicated in the schematic, a patchwork of 4 different areas on one sample was achieved: (1) background control (2) biotin only, (3) RGD and biotin and (4) RGD only. ToF-SIMS derived analysis show: (C) area scan of $C_{16}H_{11}N^-$ fragment intensities (size of image 5 mm × 5 mm, resolution: 500pixels × 500pixels) and (D) fragment signal intensities from independent spectra derived from each area. (N = 1, n = 1) (E) Streptavidin (green) bound to biotin in areas 2 and 3 was displayed by fluorescence imaging (F) HUVEC attachment to RGD in areas 3 and 4 was visualized by immunofluorescence staining of actin skeleton (white) (N = 3, n = 2).

Similarly, HUVEC seeding for 4 h in serum free condition led to evenly distributed cell attachment on areas 3 and 4, whereas cell attachment was prevented on areas 1 and 2 (Fig. 5F).

4. Discussion

By developing a versatile low-fouling PEG based coating platform

with azide functionality for biomolecule immobilization, we tailored bioactive RGD peptide concentration on substrates for controlled biological interaction such as exemplified here by endothelialization. Endothelial cell attachment and spreading were analyzed as a function of RGD concentration, and the capability of the RGD modified PEG based coating to induce an endothelium-like formation of cell layers was analyzed. Importantly, the potential of this material functionalization platform for co-immobilizing different biomolecules was demonstrated which can serve as a multifunctional biointerface in diverse applications.

Protein adsorption analysis confirmed that the here presented PAcrAm^{TM}-*g*-(PEG-N_3,NH_2,Si) coating reduced early protein adsorption from serum supplemented cell culture medium after 30 min incubation as efficiently as PAcrAm^{TM}-*g*-(PEG,NH_2,Si) (Table 1), using the same stoichiometric grafting density of 0.15 of PEG-N_3 as suggested for enhanced protein resistance by Serrano et al. [36]. Azides are small, dipolar and highly specific to alkynes for cycloaddition. Since alkynes are not found in natural proteins, the azide end groups of the PEG side chains did not alter the previously shown low-fouling properties of PAcrAm^{TM}-*g*-(PEG,NH_2,Si) [36,49,57]. Furthermore, it prevented nonspecific cell attachment in serum free conditions (Fig. 3A). However, depending on the application, for instance when in direct blood contact, further analysis of potential blood compatibility properties is required [58,59].

PAcrAm^{TM}-*g*-(PEG-N_3,NH_2,Si) enabled selective and concentration controlled immobilization of cell adhesive DBCO-RGD, as demonstrated by ToF-SIMS and VASE analysis. The immobilization followed an irreversible binding relationship as expected for this selective conjugation approach [60]. ToF-SIMS is a sensitive surface chemical analysis method, that allows detection of distinct molecular fragments on the surface of only a few nanometer (1–3 nm) depth [34,61–64]. This sensitivity enabled the surface chemical characterization of the small molecular RGD and biotin surface coatings with higher specificity and at lower concentrations than for instance X-ray photoelectron spectroscopy (XPS) (data not shown). The ToF-SIMS derived signal intensity measured in arbitrary units can be used to compare values between groups, however, computation of absolute amounts of molecules on the surface would require a good calibration curve with known surface concentrations. The measured data exhibited on average 28% standard deviation, which represents the limit of control over the exact surface concentration. The quantification of peptide layer thickness derived from VASE allowed the calculation of absolute surface concentrations according to *Eq. (1)*. A generic relationship between solution concentration and surface concentration was obtained by fitting *Eq. (2)*. The fitting revealed a maximum surface concentration of $B_{max} = 36.0\ pmol{\cdot}cm^{-2}$. For comparison, the maximum azide concentration calculated from the layer thickness of PAcrAm^{TM}-*g*-(PEG-N_3, NH_2,Si) is $c(N_3) = 38.9\ pmol{\cdot}cm^{-2}$. Since B_{max} and $c(N_3)$ are comparable, the results indicated that RGD peptide immobilization would be possible until almost complete (93%) saturation of azides without steric hindrance. At the highest used solution concentration of 100 μM, surface concentrations of $31.9 \pm 2.3\ pmol{\cdot}cm^{-2}$ and thus in average 82% of saturation of azides was achieved.

While the prevention of nonspecific attachment verified the RGD-ligand specific attachment of endothelial cells, the RGD surface concentration dependent initial cell attachment confirmed the uncompromised bioavailability of RGD after immobilization by SPAAC. This results from the highly specific cycloaddition only reacting between the azide and strained alkyne, without attacking other bonds or functionalities [48,49,57]. The range of average RGD surface concentration of 0.008 to $1.95\ pmol{\cdot}cm^{-2}$ induced changes in endothelial cell attachment. These concentrations were calculated from fitting the VASE derived data to *Eq. (2)*, since such low concentrations were below the detection limit of VASE. Similar variability as for the measured concentrations of around 28% is also expected in the here used lower concentration range. The investigated concentration range corresponded to average ligand spacings (RGD-RGD distance) of 10 to 155 nm (with expected variability of max. 20%) according to *Eq. (4)*. This range of spacings was partially overlapping with the reported range of ligand spacings of 44 to 43′700 nm on oligo-ethylene glycol passivated, RGD modified surfaces by Le Saux et al. [39], who showed the influence of those ligand densities on single endothelial cell attachment in serum free condition three hours post-seeding. The actual RGD spacings could be similar, with the discrepancy in ligand spacing ranges (10 to 155 nm or 44 to 43′700 nm) potentially deriving from different empirical methods and assumptions that lead to the estimated ligand spacing. Le Saux et al. derived the ligand distances from estimated coupling yields of RGD to oligo-ethylene glycol and from surface chemical XPS analysis, while we used layer thickness measurements derived from VASE. The positive VE-cadherin staining indicated interconnected HUVEC monolayer formation after 3 days of *in vitro* culture on RGD functionalized samples (average concentration $1.95\ pmol{\cdot}cm^{-2}$). Overall, the data provide evidence of successful steering of cellular interaction with coated biomaterials, showcased here by endothelialization. For this only low average RGD surface concentrations of $1.95\ pmol{\cdot}cm^{-2}$ are needed which corresponds to only 5% azide saturation. Importantly, this low percent of saturation leaves plenty of available azides for further functionalization. Combining several adhesion ligands, cell attachment and functionality was shown to be enhanced compared to single-molecule functionalization [65–69]. Similarly for biosensing applications co-immobilization of different molecules and thereby providing a multi-functional interface is highly desirable [70,71]. To this end, the capability of PAcrAm^{TM}-*g*-(PEG-N_3, NH_2,Si) to enable the co-immobilization of two biomolecules was explored with a model, non-cell adhesive biotin molecule.

First, the binding efficiencies of RGD and biotin should be compared. To this end, $K_{1/2}$ derived from *Eq. (2)* fitting to $C_{16}H_{11}N^-$ signal intensities were used. Lower $K_{1/2}$ for RGD $K_{1/2,ToF\text{-}SIMS,RGD} = 5.3\ \mu M$ compared to biotin ($K_{1/2,ToF\text{-}SIMS,biotin} = 54.9\ \mu M$) (also confirmed by the VASE derived $K_{1/2,VASE,RGD} = 10.6\ \mu M$) provided evidence for faster saturation compared to biotin. Since the difference is most likely not derived from steric hindrance of the larger RGD, as indicated by $B_{max,RGD,VASE}$ being close to $c(N_3)$, the difference in kinetics could thus be due to distinctive charges and polarities of the molecules [72,73], as the DBCO-RGD peptide has many charged and polar side chains such as cysteine, lysine, arginine and aspartic acid. Such differences have to be considered when using diverse active molecules for immobilization. However, overall, the selective and concentration-controlled immobilization of biomolecules was confirmed and shown to be robustly applicable to diverse biomolecules.

The availability of biotin after SPAAC immobilization was verified by an adapted ELISA assay for all analyzed biotin surface concentrations. Increasing streptavidin-HRP concentration with rising biotin concentrations confirmed the bioavailability of immobilized biotin. The relatively low concentrations of streptavidin compared to available biotin on the surface is derived from the sensitivity of the ELISA method. This observation is explored in more detail with control experiments in SI (Fig. S3). The streptavidin-HRP concentration of 0.48 nM gave a sensitive range for biotin concentrations below $0.42\ pmol{\cdot}cm^{-2}$. Above this concentration, the absorbance maximum was reached. Notably, the ELISA based method was able to confirm biotin availability in low concentration ranges of 0.002 to $0.42\ pmol{\cdot}cm^{-2}$, which were below the detection limit of the other used analytical tools (ToF-SIMS and VASE), but such RGD concentration ranges were relevant for endothelial cell interaction.

The analysis of patchwork samples with sequentially co-immobilized RGD and biotin confirmed the successful co-immobilization and their functionality. No interference between RGD and biotin, neither during the immobilization process nor during the assessment of their bioavailability was observed.

Overall, this work represents the verification of the proposed modification platform for *in vitro* cell interaction and simple biotin based

sensing on silicon oxide wafers but is only a preliminary step on the path to application in implants or biosensing. The adaptability of the modular PAcrAm^{TM} based molecule can be exploited to immobilize peptides to more application-relevant materials. For instance, it was shown that silane-based side chains form covalent bonds with different silicon-based substrate materials [36,56]. Accordingly, immobilization of PAcrAm^{TM}-*g*-(PEG-N_3,NH_2,Si) and subsequent DBCO-biotin or DBCO-RGD functionalization was possible also on glass cover slips (Fig. S5). Furthermore, the silanol side chain could be exchanged with different functionalities for steering the covalent modification of different implant materials such as titanium or different polymers [36,74].

Importantly, before considering PAcrAm^{TM}-*g*-(PEG-N_3,NH_2,Si) as potential implant surface modification or basis for biosensing, depending on the specific application, the long-term stability or degradation kinetics, long-term protein resistance, blood compatibility, cell and immune response have to be evaluated [75–77].

5. Conclusion

With the here presented results, we could underpin the robustness and versatility of our designed macromolecule PAcrAm^{TM}-*g*-(PEG-N_3, NH_2,Si). Due to the combination of different modules, a multifunctional surface coating was achieved. This stands out, compared to conventional methods, by controlled covalent and resilient surface interaction, reduced protein adsorption, and by presenting an azide functionality, the opportunity of tethering diverse biomolecules, as here shown for RGD peptide and sequentially co-immobilized biotin. This adaptability of the macromolecule combined with selective SPAAC based molecule immobilization and low-fouling background encourages the application for many different implant material concepts. Similarly, multi-modal biosensing applications that combine cell capture and/or other biomarkers from blood or other solutions could employ this multifunctional low background immobilization platform.

Data availability

The raw/processed data required to reproduce the above findings cannot be shared at this time. Raw and processed data are available from the corresponding author on reasonable request?

Funding

This research did not receive any specific grant from funding agencies in the public, commercial, or not-for-profit sectors.

CRediT authorship contribution statement

Anne-Sophie Mertgen: Conceptualization, Visualization, Investigation, Methodology, Data curation, Writing – original draft, Formal analysis. **Anne Géraldine Guex:** Conceptualization, Supervision, Writing – review & editing. **Samuele Tosatti:** Resources, Supervision, Conceptualization. **Giuseppino Fortunato:** Supervision, Writing – review & editing. **René M. Rossi:** Supervision, Writing – review & editing. **Markus Rottmar:** Conceptualization, Supervision, Writing – review & editing. **Katharina Maniura-Weber:** Conceptualization, Supervision, Writing – review & editing. **Stefan Zürcher:** Conceptualization, Methodology, Resources, Supervision, Writing – review & editing. The manuscript was written through the contributions of all authors. All authors have approved the final version of the manuscript.

Declaration of Competing Interest

The authors declare that they have no known competing financial interests or personal relationships that could have appeared to influence the work reported in this paper.

Acknowledgment

We would like to thank Prof. Dr. Viola Vogel, ETH Zurich, for valuable discussions. This work is part of the Zurich Heart project under the umbrella of University Medicine Zurich/ Hochschulmedizin Zürich.

Appendix A. Supplementary material

Supplementary data to this article can be found online at https://doi.org/10.1016/j.apsusc.2022.152525.

References

[1] A.M. Ross, J. Lahann, Current Trends and Challenges in Biointerfaces Science and Engineering, Annu. Rev. Chem. Biomol. Eng. 6 (1) (2015) 161–186, https://doi.org/10.1146/annurev-chembioeng-060713-040042.
[2] M. Kumar, R. Kumar, S. Kumar, Coatings on orthopedic implants to overcome present problems and challenges: A focused review, Mater. Today Proc. (2021). https://www.sciencedirect.com/science/article/pii/S2214785321009287.
[3] Yue Ma, Xiaohua Tian, Lei Liu, Jianming Pan, Guoqing Pan, Dynamic Synthetic Biointerfaces: From Reversible Chemical Interactions to Tunable Biological Effects, Acc. Chem. Res. 52 (6) (2019) 1611–1622, https://doi.org/10.1021/acs.accounts.8b00604.
[4] M. Pagel, A.G. Beck-Sickinger, Multifunctional biomaterial coatings: synthetic challenges and biological activity, Biol. Chem. 398 (2017) 3–22, https://doi.org/10.1515/hsz-2016-0204.
[5] Franziska Clauder, Franziska D. Zitzmann, Sabrina Friebe, Stefan G. Mayr, Andrea A. Robitzki, Annette G. Beck-Sickinger, Multifunctional coatings combining bioactive peptides and affinity-based cytokine delivery for enhanced integration of degradable vascular grafts, Biomater. Sci. 8 (6) (2020) 1734–1747, https://doi.org/10.1039/c9bm01801h.
[6] T. Liping, T. Paul, H. Wenjing, Surface Chemistry Influences Implant Biocompatibility, Curr. Top. Med. Chem. 8 (2008) 270–280, https://doi.org/10.2174/156802608783790901.
[7] X. Wang, T. Liu, Y. Chen, K. Zhang, M.F. Maitz, C. Pan, J. Chen, N. Huang, Extracellular matrix inspired surface functionalization with heparin, fibronectin and VEGF provides an anticoagulant and endothelialization supporting microenvironment, Appl. Surf. Sci. 320 (2014) 871–882, https://doi.org/10.1016/j.apsusc.2014.09.004.
[8] Peichuang Li, Zhu Luo, Xin Li, Rui Wang, Hang Chen, Yuancong Zhao, Jin Wang, Nan Huang, Preparation, evaluation and functionalization of biomimetic block copolymer coatings for potential applications in cardiovascular implants, Appl. Surf. Sci. 502 (2020) 144085, https://doi.org/10.1016/j.apsusc.2019.144085.
[9] Xiangkui Ren, Yakai Feng, Jintang Guo, Haixia Wang, Qian Li, Jing Yang, Xuefang Hao, Juan Lv, Nan Ma, Wenzhong Li, Surface modification and endothelialization of biomaterials as potential scaffolds for vascular tissue engineering applications, Chem. Soc. Rev. 44 (15) (2015) 5680–5742, https://doi.org/10.1039/C4CS00483C.
[10] Yuuki Inoue, Yuya Onodera, Kazuhiko Ishihara, Initial Cell Adhesion onto a Phospholipid Polymer Brush Surface Modified with a Terminal Cell Adhesion Peptide, ACS Appl. Mater. Interfaces. 10 (17) (2018) 15250–15257, https://doi.org/10.1021/acsami.8b0190610.1021/acsami.8b01906.s001.
[11] Won Sup Choi, Jin Woo Bae, Hye Ryeon Lim, Yoon Ki Joung, Jong-Chul Park, Il Keun Kwon, Ki Dong Park, RGD peptide-immobilized electrospun matrix of polyurethane for enhanced endothelial cell affinity, Biomed. Mater. 3 (4) (2008) 044104, https://doi.org/10.1088/1748-6041/3/4/044104.
[12] Christopher M. Kolodziej, Sung Hye Kim, Rebecca M. Broyer, Sina S. Saxer, Caitlin G. Decker, Heather D. Maynard, Combination of integrin-binding peptide and growth factor promotes cell adhesion on electron-beam-fabricated patterns, J. Am. Chem. Soc. 134 (1) (2012) 247–255, https://doi.org/10.1021/ja205524x.
[13] W. Zheng, M. Liu, H. Qi, C. Wen, C. Zhang, J. Mi, X. Zhou, L. Zhang, D. Fan, Mussel-inspired triblock functional protein coating with endothelial cell selectivity for endothelialization, J. Colloid Interface Sci. 576 (2020) 68–78, https://doi.org/10.1016/j.jcis.2020.04.116.
[14] C.J. Pan, Y.H. Hou, H.Y. Ding, Y.X. Dong, Enhancing anticoagulation and endothelial cell proliferation of titanium surface by sequential immobilization of poly(ethyleneglycol) and collagen, Appl. Surf. Sci. 287 (2013) 443–450, https://doi.org/10.1016/j.apsusc.2013.09.176.
[15] R. Konradi, M. Textor, E. Reimhult, Using complementary acoustic and optical techniques for quantitative monitoring of biomolecular adsorption at interfaces, Biosensors. 2 (2012) 341–376, https://doi.org/10.3390/bios2040341.
[16] K.L.M. Moran, J. Fitzgerald, D.A. McPartlin, J.H. Loftus, R. O'Kennedy, Biosensor-Based Technologies for the Detection of Pathogens and Toxins, in, Compr. Anal. Chem., Elsevier Ltd (2016) 93–120, https://doi.org/10.1016/bs.coac.2016.04.002.
[17] J. Xu, H. Lee, Anti-biofouling strategies for long-term continuous use of implantable biosensors, Chemosensors. 8 (2020) 1–29, https://doi.org/10.3390/chemosensors8030066.
[18] K. Qu, S.M. Kondengaden, J. Li, X. Wang, M.D. Sevilla, L. Li, X. Zeng, Carbohydrate-functionalized polythiophene biointerface: design, fabrication, characterization and application for protein analysis, Appl. Surf. Sci. 486 (2019) 561–570, https://doi.org/10.1016/j.apsusc.2019.04.231.

[19] Patricia C. Weber, D.H. Ohlendorf, J.J. Wendoloski, F.R. Salemme, Structural Origins of High-Affinity Biotin Binding to Streptavidin, Science 243 (4887) (1989) 85–88, https://doi.org/10.1126/science.2911722.

[20] Yifei Li, Haining Zhang, Binding of Streptavidin to Surface-attached Biotin with Different Spacer Thicknesses, J. Wuhan Univ. Technol. Sci. Ed. 30 (6) (2015) 1304–1309, https://doi.org/10.1007/s11595-015-1312-5.

[21] L. Pol, C. Eckstein, L. Acosta, E. Xifré-Pérez, J. Ferré-Borrull, L. Marsal, Real-Time Monitoring of Biotinylated Molecules Detection Dynamics in Nanoporous Anodic Alumina for Bio-Sensing, Nanomaterials. 9 (2019) 478, https://doi.org/10.3390/nano9030478.

[22] D.L. Hern, J.A. Hubbell, Incorporation of adhesion peptides into nonadhesive hydrogels useful for tissue resurfacing, J. Biomed. Mater. Res. 39 (1998) 266–276, https://doi.org/10.1002/(SICI)1097-4636(199802)39:2%3C266::AID-JBM14%3E3.0.CO;2-B.

[23] Danielle S.W. Benoit, Kristi S. Anseth, The effect on osteoblast function of colocalized RGD and PHSRN epitopes on PEG surfaces, Biomaterials. 26 (25) (2005) 5209–5220, https://doi.org/10.1016/j.biomaterials.2005.01.045.

[24] M. Schuler, G.R. Owen, D.W. Hamilton, M. de Wild, M. Textor, D.M. Brunette, S.G. P. Tosatti, G. Rh, D.W. Hamilton, M. De Wild, M. Textor, D.M. Brunette, S.G. P. Tosatti, Biomimetic modification of titanium dental implant model surfaces using the RGDSP-peptide sequence: A cell morphology study, Biomaterials. 27 (2006) 4003–4015, https://doi.org/10.1016/j.biomaterials.2006.03.009.

[25] S. Tosatti, S.M. De Paul, A. Askendal, S. VandeVondele, J.A. Hubbell, P. Tengvall, M. Textor, Peptide functionalized poly(l-lysine)-g-poly(ethylene glycol) on titanium: resistance to protein adsorption in full heparinized human blood plasma, Biomaterials. 24 (27) (2003) 4949–4958, https://doi.org/10.1016/S0142-9612(03)00420-4.

[26] S. VandeVondele, J. Vörös, J.A. Hubbell, RGD-grafted poly-L-lysine-graft-(polyethylene glycol) copolymers block non-specific protein adsorption while promoting cell adhesion, Biotechnol. Bioeng. 82 (2003) 784–790, https://doi.org/10.1002/bit.10625.

[27] Yan-Yan Wang, Lan-Xin Lü, Jun-Cai Shi, Hai-Feng Wang, Zhong-Dang Xiao, Ning-Ping Huang, Introducing RGD peptides on PHBV films through PEG-containing cross-linkers to improve the biocompatibility, Biomacromolecules. 12 (3) (2011) 551–559, https://doi.org/10.1021/bm100886w.

[28] Qiang Wei, Tobias Becherer, Stefano Angioletti-Uberti, Joachim Dzubiella, Christian Wischke, Axel T. Neffe, Andreas Lendlein, Matthias Ballauff, Rainer Haag, Protein Interactions with Polymer Coatings and Biomaterials, Angew. Chemie Int. Ed. 53 (31) (2014) 8004–8031, https://doi.org/10.1002/anie.201400546.

[29] Li-Chong Xu, Christopher A. Siedlecki, Protein adsorption, platelet adhesion, and bacterial adhesion to polyethylene-glycol-textured polyurethane biomaterial surfaces, J. Biomed. Mater. Res. - Part B Appl. Biomater. 105 (3) (2017) 668–678, https://doi.org/10.1002/jbm.b.33592.

[30] V.B. Damodaran, S.N. Murthy, Bio-inspired strategies for designing antifouling biomaterials, Biomater. Res. 20 (2016) 18, https://doi.org/10.1186/s40824-016-0064-4.

[31] Shenfu Chen, Lingyan Li, Chao Zhao, Jie Zheng, Surface hydration: Principles and applications toward low-fouling/nonfouling biomaterials, Polymer (Guildf). 51 (23) (2010) 5283–5293, https://doi.org/10.1016/j.polymer.2010.08.022.

[32] Chuan Leng, Hsiang-Chieh Hung, Shuwen Sun, Dayang Wang, Yuting Li, Shaoyi Jiang, Zhan Chen, Probing the Surface Hydration of Nonfouling Zwitterionic and PEG Materials in Contact with Proteins, ACS Appl. Mater. Interfaces. 7 (30) (2015) 16881–16888, https://doi.org/10.1021/acsami.5b05627.

[33] Marta Cerruti, Stefano Fissolo, Carlo Carraro, Carlo Ricciardi, Arun Majumdar, Roya Maboudian, Poly(ethylene glycol) monolayer formation and stability on gold and silicon nitride substrates, Langmuir. 24 (19) (2008) 10646–10653, https://doi.org/10.1021/la801357v.

[34] S. Pasche, S.M. De Paul, J. Vörös, N.D. Spencer, M. Textor, Poly (L-lysine)-graft-poly(ethylene glycol) Assembled Monolayers on Niobium Oxide Surfaces: A Quantitative Study of the Influence of Polymer Interfacial Architecture on Resistance to Protein Adsorption by ToF-SIMS and In Situ OWLS, Langmuir. 19 (2003) 9216–9225, https://doi.org/10.1021/la034111y.

[35] D.L. Elbert, J.A. Hubbell, Reduction of fibrous adhesion formation by a copolymer possessing an affinity for anionic surfaces, J. Biomed. Mater. Res. 42 (1998) 55–65, https://doi.org/10.1002/(SICI)1097-4636(199810)42:1<55::AID-JBM8>3.0.CO;2-N.

[36] Ângela Serrano, Stefan Zürcher, Samuele Tosatti, Nicholas D. Spencer, Imparting Nonfouling Properties to Chemically Distinct Surfaces with a Single Adsorbing Polymer: A Multimodal Binding Approach, Macromol. Rapid Commun. 37 (7) (2016) 622–629, https://doi.org/10.1002/marc.201500683.

[37] Roger Michel, Stephanie Pasche, Marcus Textor, David G. Castner, Influence of PEG architecture on protein adsorption and conformation, Langmuir. 21 (26) (2005) 12327–12332, https://doi.org/10.1021/la051726h.

[38] G.L. Kenausis, J. Vörös, D.L. Elbert, N. Huang, R. Hofer, L. Ruiz-Taylor, M. Textor, J.A. Hubbell, N.D. Spencer, Poly(l-lysine)-g-Poly(ethylene glycol) Layers on Metal Oxide Surfaces: Attachment Mechanism and Effects of Polymer Architecture on Resistance to Protein Adsorption, J. Phys. Chem. B. 104 (2002) 3298–3309, https://doi.org/10.1021/jp993359m.

[39] Guillaume Le Saux, Astrid Magenau, Krishanthi Gunaratnam, Kristopher A. Kilian, Till Böcking, J.Justin Gooding, Katharina Gaus, Spacing of integrin ligands influences signal transduction in endothelial cells, Biophys. J. 101 (4) (2011) 764–773, https://doi.org/10.1016/j.bpj.2011.06.064.

[40] Xin Wang, Stuart Cooper, Adhesion of endothelial cells and endothelial progenitor cells on peptide-linked polymers in shear flow, Tissue Eng Part A. 19 (9-10) (2013) 1113–1121, https://doi.org/10.1089/ten.TEA.2011.0653.

[41] Christopher D. Spicer, E. Thomas Pashuck, Molly M. Stevens, Achieving Controlled Biomolecule-Biomaterial Conjugation, Chem. Rev. 118 (16) (2018) 7702–7743, https://doi.org/10.1021/acs.chemrev.8b00253.

[42] Julia Morales-Sanfrutos, Javier Lopez-Jaramillo, Mariano Ortega-Muñoz, Alicia Megia-Fernandez, Francisco Perez-Balderas, Fernando Hernandez-Mateo, Francisco Santoyo-Gonzalez, Vinyl sulfone: A versatile function for simple bioconjugation and immobilization, Org. Biomol. Chem. 8 (3) (2010) 667–675, https://doi.org/10.1039/b920576d.

[43] Shunsuke Chatani, Devatha P. Nair, Christopher N. Bowman, Relative reactivity and selectivity of vinyl sulfones and acrylates towards the thiol-Michael addition reaction and polymerization, Polym. Chem. 4 (4) (2013) 1048–1055, https://doi.org/10.1039/c2py20826a.

[44] Rainer Bischoff, Hartmut Schlüter, Amino acids: Chemistry, functionality and selected non-enzymatic post-translational modifications, J. Proteomics. 75 (8) (2012) 2275–2296, https://doi.org/10.1016/j.jprot.2012.01.041.

[45] Matt J. Kipper, Hynda K. Kleinman, Francis W. Wang, Covalent surface chemistry gradients for presenting bioactive peptides, Anal. Biochem. 363 (2) (2007) 175–184, https://doi.org/10.1016/j.ab.2007.01.036.

[46] Hyun Jong Lee, Gabriella M. Fernandes-Cunha, Ilham Putra, Won-Gun Koh, David Myung, Tethering Growth Factors to Collagen Surfaces Using Copper-Free Click Chemistry: Surface Characterization and in Vitro Biological Response, ACS Appl. Mater. Interfaces. 9 (28) (2017) 23389–23399, https://doi.org/10.1021/acsami.7b05262.

[47] Marjoke F. Debets, Sander S. van Berkel, Jan Dommerholt, A. (Ton) J. Dirks, Floris P.J.T. Rutjes, Floris L. van Delft, Bioconjugation with strained alkenes and alkynes, Acc. Chem. Res. 44 (9) (2011) 805–815, https://doi.org/10.1021/ar200059z.

[48] Ngalle Eric Mbua, Jun Guo, Margreet A. Wolfert, Richard Steet, Geert-Jan Boons, Strain-Promoted Alkyne – Azide Cycloadditions (SPAAC) Reveal New Features of Glycoconjugate Biosynthesis, ChemBioChem. 12 (12) (2011) 1912–1921, https://doi.org/10.1002/cbic.201100117.

[49] J. Dommerholt, F.P.J.T. Rutjes, F.L. Van Delft, Strain-Promoted 1,3-Dipolar Cycloaddition of Cycloalkynes and Organic Azides, Top. Curr. Chem. 374 (2016) 1–20, https://doi.org/10.1007/s41061-016-0016-4.

[50] Stijn F.M. van Dongen, Paolo Maiuri, Emmanuelle Marie, Christophe Tribet, Matthieu Piel, Triggering cell adhesion, migration or shape change with a dynamic surface coating, Adv. Mater. 25 (12) (2013) 1687–1691, https://doi.org/10.1002/adma.201204474.

[51] B.H. Chick, C.J. Martin, The Density and Solution Volume of Some Proteins, Biochem. J. 7 (1913) 92–96, https://doi.org/10.1042/bj0070092.

[52] E. Berlin, M.J. Pallansch, Densities of several proteins and L-amino acids in the dry state, J. Phys. Chem. 72 (6) (1968) 1887–1889, https://doi.org/10.1021/j100852a004.

[53] H. Fischer, I. Polikarpov, A.F. Craievich, Average protein density is a molecular-weight-dependent function, Protein Sci. 13 (2004) 2825–2828, https://doi.org/10.1110/ps.04688204.studies.

[54] S. Saxer, C. Portmann, S. Tosatti, K. Gademann, S. Zürcher, M. Textor, Surface assembly of catechol-functionalized poly(L-lysine)-graft-poly(ethylene glycol) copolymer on titanium exploiting combined electrostatically driven self-organization and biomimetic strong adhesion, Macromolecules. 43 (2010) 1050–1060, https://doi.org/10.1021/ma9020664.

[55] Yizhi Liang, Smita S. Patel, Donald H. Dean, Irreversible binding kinetics of Bacillus thuringiensis CryIA δ-endotoxins to gypsy moth brush border membrane vesicles is directly correlated to toxicity, J. Biol. Chem. 270 (42) (1995) 24719–24724, https://doi.org/10.1074/jbc.270.42.24719.

[56] Serge Weydert, Stefan Zürcher, Stefanie Tanner, Ning Zhang, Rebecca Ritter, Thomas Peter, Mathias J. Aebersold, Greta Thompson-Steckel, Csaba Forró, Markus Rottmar, Flurin Stauffer, Irene A. Valassina, Giulia Morgese, Edmondo M. Benetti, Samuele Tosatti, János Vörös, Easy to Apply Polyoxazoline-Based Coating for Precise and Long-Term Control of Neural Patterns, Langmuir. 33 (35) (2017) 8594–8605, https://doi.org/10.1021/acs.langmuir.7b0143710.1021/acs.langmuir.7b01437.s001.

[57] A. Kuzmin, A. Poloukhtine, M.A. Wolfert, V.V. Popik, Surface Functionalization Using Catalyst-Free Azide - Alkyne Cycloaddition, Bioconjug. Chem. 21 (2010) 2076–2085, https://doi.org/10.1021/bc100306u.

[58] M. Weber, H. Steinle, S. Golombek, L. Hann, C. Schlensak, H.P. Wendel, M. Avci-Adali, Blood-Contacting Biomaterials. In Vitro Evaluation of the Hemocompatibility, Front. Bioeng. Biotechnol. 6 (2018), https://doi.org/10.3389/fbioe.2018.00099.

[59] J.L. Brash, T.A. Horbett, R.A. Latour, P. Tengvall, The blood compatibility challenge. Part 2: Protein adsorption phenomena governing blood reactivity, Acta Biomater. 94 (2019) 11–24, https://doi.org/10.1016/j.actbio.2019.06.022.

[60] E.C. Hulme, M.A. Trevethick, Ligand binding assays at equilibrium: validation and interpretation, Br. J. Pharmacol. 161 (2010) 1219–1237, https://doi.org/10.1111/j.1476-5381.2009.00604.x.

[61] Laetitia Bernard, Patrick Rupper, Greta Faccio, Dirk Hegemann, Olivier Scholder, Manfred Heuberger, Katharina Maniura-Weber, Marianne Vandenbossche, Plasma polymer film designs through the eyes of ToF-SIMS, Biointerphases. 13 (3) (2018) 03B417, https://doi.org/10.1116/1.5016046.

[62] Timothy J. Barnes, Ivan M. Kempson, Clive A. Prestidge, Surface analysis for compositional, chemical and structural imaging in pharmaceutics with mass spectrometry: A ToF-SIMS perspective, Int. J. Pharm. 417 (1-2) (2011) 61–69, https://doi.org/10.1016/j.ijpharm.2011.01.043.

[63] S.C. Youn, L.Y. Chen, R.J. Chiou, T.J. Lai, W.C. Liao, F. Der Mai, H.M. Chang, Comprehensive Application of Time-of-flight Secondary Ion Mass Spectrometry (TOF-SIMS) for Ionic Imaging and Bio-energetic Analysis of Club Drug-induced

Cognitive Deficiency, Sci. Rep. 5 (2015) 18420, https://doi.org/10.1038/srep18420.
[64] S. Roberson, A. Sehgal, A. Fahey, A. Karim, Time-of-flight secondary ion mass spectrometry (TOF-SIMS) for high-throughput characterization of biosurfaces, Appl. Surf. Sci. 203–204 (2003) 855–858, https://doi.org/10.1016/S0169-4332(02)00822-X.
[65] Zhen-Yu Guan, Chih-Yu Wu, Jyun-Ting Wu, Ching-Heng Tai, Jiashing Yu, Hsien-Yeh Chen, Multifunctional and Continuous Gradients of Biointerfaces Based on Dual Reverse Click Reactions, ACS Appl. Mater. Interfaces. 8 (22) (2016) 13812–13818, https://doi.org/10.1021/acsami.6b0390810.1021/acsami.6b03908.s001.
[66] Hyun Ki Min, Se Heang Oh, Jong Min Lee, Gun Il Im, Jin Ho Lee, Porous membrane with reverse gradients of PDGF-BB and BMP-2 for tendon-to-bone repair: In vitro evaluation on adipose-derived stem cell differentiation, Acta Biomater. 10 (3) (2014) 1272–1279, https://doi.org/10.1016/j.actbio.2013.12.031.
[67] Yanrui Ma, Gina M. Policastro, Qiyao Li, Jukuan Zheng, Robin Jacquet, William J. Landis, Matthew L. Becker, Concentration-Dependent hMSC Differentiation on Orthogonal Concentration Gradients of GRGDS and BMP-2 Peptides, Biomacromolecules. 17 (4) (2016) 1486–1495, https://doi.org/10.1021/acs.biomac.6b0008810.1021/acs.biomac.6b00088.s001.
[68] Douglas Zhang, Kristopher A. Kilian, Peptide microarrays for the discovery of bioactive surfaces that guide cellular processes: a single step azide–alkyne “click” chemistry approach, J. Mater. Chem. B. 2 (27) (2014) 4280–4288, https://doi.org/10.1039/c4tb00375f.
[69] Anne-Sophie Mertgen, Vanessa Tanja Trossmann, Anne Géraldine Guex, Katharina Maniura-Weber, Thomas Scheibel, Markus Rottmar, Multifunctional Biomaterials: Combining Material Modification Strategies for Engineering of Cell-Contacting Surfaces, ACS Appl. Mater. Interfaces. 12 (19) (2020) 21342–21367, https://doi.org/10.1021/acsami.0c01893.
[70] Subramanian Tamil Selvan, Timothy Thatt Yang Tan, Dong Kee Yi, Nikhil R. Jana, Functional and multifunctional nanoparticles for bioimaging and biosensing, Langmuir. 26 (14) (2010) 11631–11641, https://doi.org/10.1021/la903512m.
[71] H.D.M. Follmann, A.F. Naves, R.A. Araujo, V. Dubovoy, X. Huang, T. Asefa, R. Silva, O.N. Oliveira, Hybrid Materials and Nanocomposites as Multifunctional Biomaterials, Curr. Pharm. Des. 23 (2017) 3794–3813, https://doi.org/10.2174/1381612823666170710160615.
[72] P. Comeau, T. Willett, Impact of Side Chain Polarity on Non-Stoichiometric Nano-Hydroxyapatite Surface Functionalization with Amino Acids, Sci. Rep. 8 (2018) 12700, https://doi.org/10.1038/s41598-018-31058-5.
[73] Chad J. Pickens, Stephanie N. Johnson, Melissa M. Pressnall, Martin A. Leon, Cory J. Berkland, Practical Considerations, Challenges, and Limitations of Bioconjugation via Azide − Alkyne Cycloaddition, Bioconjug. Chem. 29 (3) (2018) 686–701, https://doi.org/10.1021/acs.bioconjchem.7b00633.
[74] Olof Sterner, Marta Giazzon, Stefan Zürcher, Samuele Tosatti, Martha Liley, Nicholas D. Spencer, Delineating fibronectin bioadhesive micropatterns by photochemical immobilization of polystyrene and poly(vinylpyrrolidone), ACS Appl. Mater. Interfaces. 6 (21) (2014) 18683–18692, https://doi.org/10.1021/am5042093.
[75] Friedrich Jung, Steffen Braune, Thrombogenicity and hemocompatibility of biomaterials, Biointerphases. 11 (2) (2016) 029601, https://doi.org/10.1116/1.4938557.
[76] D. Karpman, A. Ståhl, I. Arvidsson, K. Johansson, S. Loos, R. Tati, Z. Békássy, A. Kristoffersson, M. Mossberg, R. Kahn, Complement Interactions with Blood Cells, Endothelial Cells and Microvesicles in Thrombotic and Infl ammatory Conditions Diana, in: Immune Responses to Biosurfaces, Springer International Publishing Switzerland, 2015: pp. 19–42. https://doi.org/10.1007/978-3-319-18603-0.
[77] P. Thevenot, W. Hu, L. Tang, T. Liping, T. Paul, H. Wenjing, Surface chemistry influences implant biocompatibility, Curr. Top. Med. Chem. 8 (2008) 270–280, https://doi.org/10.2174/156802608783790901.